Elastic-Viscoplastic Finite-Element Program for Modeling Tire/Soil Interaction

Joseph E. Saliba*
University of Dayton, Dayton, Ohio

The viscoplastic finite-element program for modeling tire/soil interaction is shown to be a powerful analytical tool that has a significant promise for improving the Air Force ability to predict aircraft ground operation. A brief review of the mathematical theory of viscoplasticity and the computational procedure used in the finite-element program is first presented. Next, some of the capabilities of this powerful analytical tool are demonstrated. The first example considered is that of the effect of tire pressure on sinkage and rut depth produced on constant strength clay and sand soils. Then, the effect of layered soil on sinkage and rut depth is examined, considering the possibility of soft over hard as well as of hard over soft layers. This latest case is further studied investigating the effect of the variation of the top thickness layer on sinkage. In conclusion, tables are presented that provide an equivalent cone index for a two-layered clay soil of different strengths and thicknesses. To demonstrate the capability of the program to model contingency surfaces, the behavior of standard flexible and rigid pavements under a medium tire pressure were considered.

I. Introduction

READINESS and survivability, important United States Air Force (USAF) objectives for nonstrategic forces, must be achieved in the key area of sortie generation. Critical elements in obtaining rapid and sustained sortie generation are aircraft launch and recovery, where current and long-range actions are providing improvements. The effective development, optimization, and application of many of these actions depend upon reliably predicting aircraft capability to operate on various ground surfaces.

Most USAF aircraft were designed for operation on high-strength, smooth, paved surfaces making these surfaces high priority wartime targets and subject to damage. Reliable prediction techniques exist for aircraft operation on conventional pavement surfaces. However, validated techniques are not yet available for predicting aircraft operation on soil or any other contingency/austere ground surfaces.

In the past two decades, the USAF accomplished a number of research efforts resulting in computer programs which simulate the operation of aircraft on soils.[1-5] These programs are only valid for constant strength media restricting simulation capabilities over layered soils. To remedy this problem, a viscoplastic finite-element program[6] was developed to correlate layered soil or other layered surfaces to single strength media. But such a program can be much more useful than as a correlation tool only. For example, it can be applied to compute the sinkage and rut-depth profiles under a tire or the variation of pressure or stress with depth.

II. Objective

The objective of this study was to demonstrate the capabilities of the viscoplastic finite-element computer program to predict sinkage and rut depth, which can later be used as input data to existing routines that simulate aircraft operating on soil and other contingency/austere ground surfaces. The tasks pursued to achieve the objective were to 1) summarize the mathematical theory of viscoplasticity and the computational procedure used in the finite-element program; 2) use the program to compute sinkage and rut depth due to low-, medium-, and high-pressure tire travel over constant strength, single layer clay and silty sand type soils; 3) predict sinkage and rut depth for tire travel over layered soil and study the effect of top layer thickness; 4) compute an equivalent cone index for a two-layered soil of different strength and thicknesses for an F-4 tire; and 5) predict sinkage and rut depth for tire travel over flexible and rigid pavements.

III. Mathematical Theory of Viscoplasticity

A. General

The elastoviscoplastic theory[7] is based on the assumption that the total strain rate is divided into two parts

$$\dot{\epsilon} = \dot{\epsilon}_e + \epsilon_{vp} \tag{1}$$

where $(\dot{})$ is the differentiation with respect to time; ϵ, ϵ_e, and ϵ_{vp} are the total, elastic, and viscoplastic strain, respectively.

The total stress σ can then be written as

$$\sigma = D\epsilon_e \tag{2}$$

where D is the elasticity matrix.

The viscoplastic behavior is dictated by a scalar yield criterion

$$F(\sigma,\epsilon_{vp}) - F_0 = 0 \tag{3}$$

in which F_0 is the uniaxial yield stress, which may itself be a function of the state of the material. With $F < F_0$, a purely elastic behavior will occur; with $F > F_0$, a viscoplastic behavior is assumed.

To define the relationship between the various strain components, we borrow from the classical plasticity theory, the idea of a plastic potential, denoted herein by $Q(\sigma)$

$$\dot{\epsilon}_{vp} = \gamma\langle\Phi(F)\rangle \frac{\partial Q}{\partial \sigma} \tag{4}$$

where ∂/∂ is the partial derivative, γ is a fluidity parameter controlling the plastic flow rate, $\Phi(F)$ is a positive monotoni-

Received Nov. 19, 1988; revision received Sept. 15, 1989.

*Associate Professor, Department of Civil Engineering and Engineering Mechanics.

cally increasing function for $F>0$, and $\langle\Phi(F)\rangle$ is equal to $\Phi(F)$ for $F>0$ or $=0$ for $F\leq 0$. If $F=Q$, then the flow rule is of the associated kind. If $F\neq Q$, then the flow rule is said to be nonassociated. We can rewrite Eq. (4) as

$$\dot{\epsilon}_{vp}=\gamma\langle\Phi(F)\rangle\frac{\partial Q}{\partial\sigma}=\gamma\langle\Phi\rangle\boldsymbol{a} \tag{5}$$

where vector $\boldsymbol{a}=\partial Q/\partial\sigma$.

B. Viscoplastic Strain Increment

Kanchi et al.[8] suggested using a parameterized time-stepping scheme to define a strain increment $(\Delta\epsilon_{vp})_n$ occurring in a time interval $\Delta T_n=t_{n+1}-t_n$ as

$$\Delta\epsilon_{vp}^n=\Delta t_n\left[(1-\alpha)\dot{\epsilon}_{vp}^n+\alpha\dot{\epsilon}_{vp}^{n+1}\right] \tag{6a}$$

To complete $\dot{\epsilon}_{vp}^{n+1}$ in Eq. (6a), we could use a simplified Taylor series expansion

$$\dot{\epsilon}_{vp}^{n+1}=\dot{\epsilon}_{vp}^n+H^n\Delta\sigma^n \tag{6b}$$

where

$$H^n=\left(\frac{\partial\dot{\epsilon}_{vp}}{\partial\sigma}\right)=H^n(\sigma^n)$$

and $\Delta\sigma^n$ is the stress increment in the time interval Δt^n. Rewriting Eqs. (6)

$$\Delta\epsilon_{vp}^n=\dot{\epsilon}_{vp}^n\Delta t_m+C^n\Delta\sigma^m \tag{6c}$$

where

$$C^n=\alpha\Delta t_m H^n$$

A fully explicit method can be obtained if α is set to 0. A fully implicit scheme results if α is set to 1. An implicit trapezoidal or Crank-Nicolson rule will be obtained if $\alpha=\frac{1}{2}$.

C. Stress Increments

Using an incremental form of Eq. (2), we obtain

$$\Delta\sigma^n=D\Delta\epsilon_e^n=D(\Delta\epsilon^n-\Delta\epsilon_{vp}^n) \tag{7}$$

By expressing the total strain increment in terms of the displacement increment as

$$\Delta\epsilon^n=B^n\Delta d^n \tag{8}$$

where B is the nodal strain displacement operator matrix and Δd the incremental displacement. Substituting Eqs. (6c) and (8) into Eq. (7), we can write

$$\Delta\sigma^n=\hat{D}^n(B^n\Delta d^n-\epsilon_{vp}\Delta t_n) \tag{9}$$

where

$$\hat{D}^n=(I+DC^n)^{-1}D=(D^{-1}+C^n)^{-1} \tag{10}$$

The B^n is substituted for B because of the possibility that the strain matrix may vary throughout the solution. In case of large deformation, which can easily occur in soft soil, the strain matrix for a Lagrangian formulation is nonlinear and can be written as

$$B^n=B_0+B_{NL}^n$$

where B_0 represents the standard linear terms which do not vary during the solution, and B_{NL}^n contains the nonlinear quadratic terms.

D. Equations of Equilibrium

The force equilibrium equation at time t_n over the complete domain is

$$\int_\Omega[B^n]^T\sigma^n\,d\Omega+f^n=0 \tag{11}$$

where f^n is a vector containing applied nodal surface tractions, body forces, thermal loads, etc. During a time increment, the equilibrium equation can then be written as

$$\int_\Omega[B^n]^T\Delta\sigma^n\,d\Omega+\Delta f^n=0 \tag{12}$$

where Δf^n is the change in applied nodal loads during the time interval Δt_n.

The tangential stiffness matrix can be computed by replacing the elasticity matrix D by $\hat{D}^n$ in the regular formulation of the elastic problem; thus, we have

$$K_T^n=\int_\Omega[B^n]^T\hat{D}^nB^n\,d\Omega \tag{13}$$

Using Eqs. (12) and (13), we can state that

$$\Delta d^n=[K_T^n]^{-1}\Delta V^n \tag{14}$$

where

$$\Delta V^n=\int_\Omega[B^n]^T\Delta\sigma^n\,d\Omega+\Delta f^n$$

Replacing $\Delta\sigma^n$ by Eq. (9), we obtain

$$\Delta V^n=\int_\Omega[B^n]^T\hat{D}^n\dot{\epsilon}_{vp}^n\Delta t_n\,d\Omega+\Delta f^n \tag{15}$$

The ΔV^n are called the incremental pseudoloads. Stricklin et al.[9] suggested computing the residual forces Ψ as

$$\Psi^{n+1}+\int_\Omega[B^{n+1}]^T\sigma^{n+1}\,d\Omega+f^{n+1}\neq 0 \tag{16}$$

The residual force is then added to the applied nodal force increment at the next time step, thus avoiding an iteration process and at the same time reducing the error propagation.

E. Yield Criteria for Soil

The failure of a soil mass seems to be in accordance with the tenets of the Mohr theory of failure.

The Mohr-Coulomb yield surface (see Fig. 1) defined in

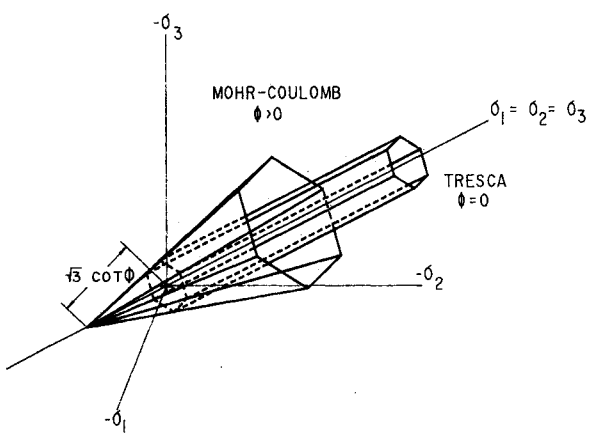

Fig. 1 Mohr-Coulomb yield locus.

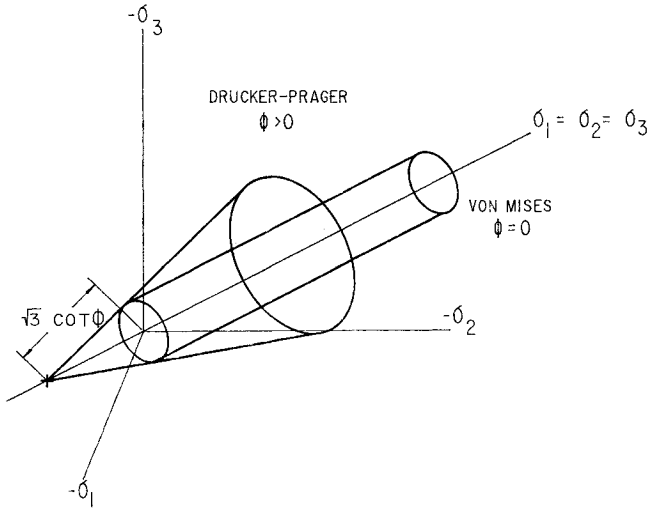

Fig. 2 Drucker-Prager yield locus.

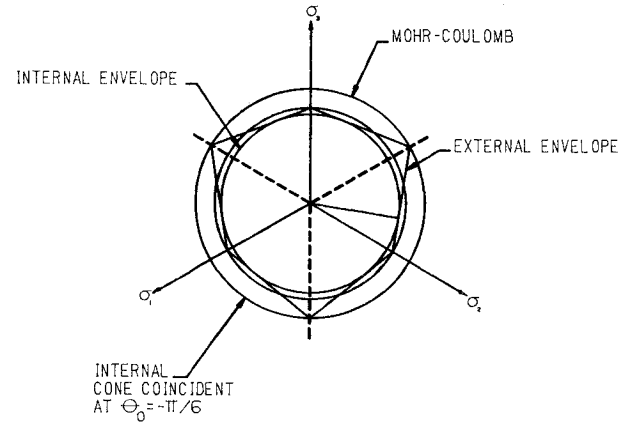

Fig. 3 Plane of the Drucker-Prager and Mohr-Coulomb criteria.

terms of the stress invariants, $\sigma_m = J_1/3$, J_2, and the Lode angle Θ_0 can be written as

$$F = \sigma_m \sin\phi + \sqrt{J_2}\cos\Theta_0 - \frac{\sqrt{J_2}}{\sqrt{3}}\sin\Theta_0 \sin\phi - c\cos\phi \qquad (17)$$

where c is the cohesion factor and ϕ the friction angle.[7]

The yield surfaces defined in the preceding section have a serious drawback due to their angular nature in the principal stress space. Whenever stresses are such that they fail on one of the "ridges" of the yield surfaces, the directions of derivatives are not unique.

If the Mohr-Coulomb surface is to be represented by a circular cone, which one would represent the angular surface best? There are an infinite number of cones which could be chosen. One example is the Drucker-Prager,[7] which can be written as

$$F = \frac{6\sin\sigma m}{\sqrt{3}(3-\sin\phi)} + \sqrt{J_2} - \frac{6c\cos\phi}{\sqrt{3}(3-\sin\phi)} \qquad (18)$$

which represents a cone passing through the exterior corners of the Mohr-Coulomb pyramid (see Figs. 2 and 3).

F. Computational Procedure

The computational procedure is divided into six major steps.

1) Suppose at time $t = t_n$ we have an equilibrium situation and d^n, σ^n, ϵ^n, ϵ^n_{vp}, F^n are known. The following quantities are assembled:

a) $B^n = B_0 + B_{NL}(d^n)$ where $B_{NL}(d^n)$ is the nonlinear term of the strain matrix
b) $C^n = C^n(\sigma^n, \Delta t_n)$,
c) $D^n = (D^{-1} + C^n)^{-1}$,
d) $K^n_T = \int_\Omega [B^n]^T \hat{D}^n B^n \, d\Omega$, and
e) $\dot{\epsilon}^n_{vp} = \gamma\langle\Phi\rangle a^n$.

Once all of the above are computed, then proceed to

2) Compute the displacement increments Δd^n from Eq. (14)

$$\Delta d^n = [K^n_T]^{-1}\Delta V^n$$

where

$$\Delta V^n = \int_\Omega [B^n]^T \hat{D}^n \dot{\epsilon}^n_{vp} \Delta t_n \, d\Omega + \Delta f^n$$

Compute the stress increment $\Delta\sigma^n$ as

$$\Delta\sigma^n = \hat{D}^n(B^n \Delta d^n - \dot{\epsilon}^n_{vp}\Delta t_n)$$

3) Compute the total displacements and stresses

$$d^{n+1} = d^n + \Delta d^n$$

$$\sigma^{n+1} = \sigma^n + \Delta\sigma^n$$

4) Update the viscoplastic strain rate

$$\dot{\epsilon}^{n+1}_{vp} = \gamma\langle\Phi\rangle a^{n+1}$$

5) Apply the equilibrium correction equation [Eq. (16)] and add it to the incremental pseudoloads for use in the next time step.

6) Check if a steady state has been reached at each of the integration points in each element. If so, the solution is terminated or the next load increment is applied or return to step 1 and repeat for the next time step.

It has been shown[10] that the generalized one parameter family of implicit integration schemes which apply to both associated and nonassociated flow rules and to any smooth yield function are unconditionally stable numerically for the value of that parameter larger than or equal to one-half.

IV. Effect of Tire Pressure on Constant Strength Soil Sinkage and Rut Depth

Sinkage is the instantaneous deformation or the distance between the undisturbed soil surface and the bottom of the tire. Rut depth is defined as the distance between the original ground surface and rut-bottom elevations after a tire has passed over the surface and the soil rebound has been completed.

The program was used to compute tire sinkage and rut depth due to low-, medium-, and high-pressure tires traveling over two types of constant strength single layer soils shown in Table 1.

The fluidity parameter used is arbitrary since we are interested in the steady-state solution. Thus we are neglecting the effect of the load rate, making this analysis valid only for very low speed (less than 5 mph) or quasistatic cases. The strip of soil lies in a plane perpendicular to the long axis of the footprint. Only half of the strip is modeled, taking advantage of the symmetry in the problem. The finite-element model with all of the geometry and the three different pressure distributions are shown in Fig. 4.

The semi-infinite boundary problem effect was checked and found to be much smaller than the error expected in these typical soil problems. Also, the convergence was examined by refining the model shown in Fig. 4.

A state of plane strain is assumed, and the Mohr-Coulomb yield function is chosen to predict yielding. Associated flow rule is assumed for clay, and nonassociated flow is considered to model the viscoplastic flow rate for sand. When the nonas-

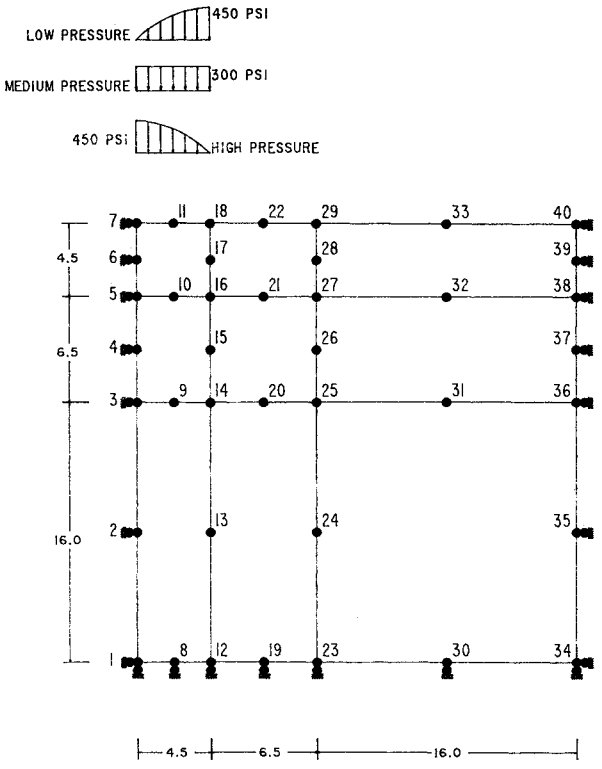

Fig. 4 Constant strength finite-element model.

Table 1 Material properties for single layer soil pavement

Material properties	Clay	Silty sand
Modulus of elasticity, psi	500	15,000
Poisson's ratio	0.3	0.3
Cohesion factor, psi	5.0	1.0
Friction angle, deg	0.0	25.0
Fluidity parameter, 1/s	0.05	0.05

Table 2 Material properties for layered soil pavement

	Clay		Sand	
Material properties	Soft	Hard	Soft	Hard
Modulus of elasticity, psi	4500	10,000	7000	30,000
Poisson's ratio	0.3	0.3	0.3	0.3
Cohesion factor, psi	3.0	6.0	0.5	2.0
Friction angle, deg	0.0	0.0	20.0	20.0
Fluidity parameter, 1/s	0.05	0.05	0.05	0.5

Table 3 Material properties for rigid and flexible pavements

Material properties	Asphalt/Portland cement/concrete	Crushed stone	Clay
Modulus of elasticity, psi	15,000/240,000	50,000	3000
Poisson's ratio	0.3/0.15	0.3	0.3
Cohesion factor, psi	10.0/990	25.0	3.0
Friction angle, deg	0.0/0.0	45.0	0.0
Fluidity parameter, 1/s	0.05/0.05	0.05	0.05

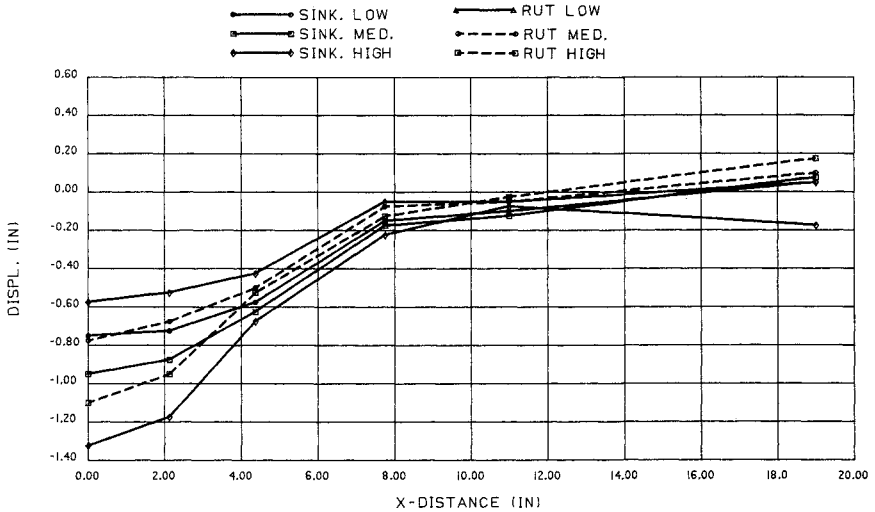

Fig. 5 Sinkage and rut depth for three tire pressures on clay.

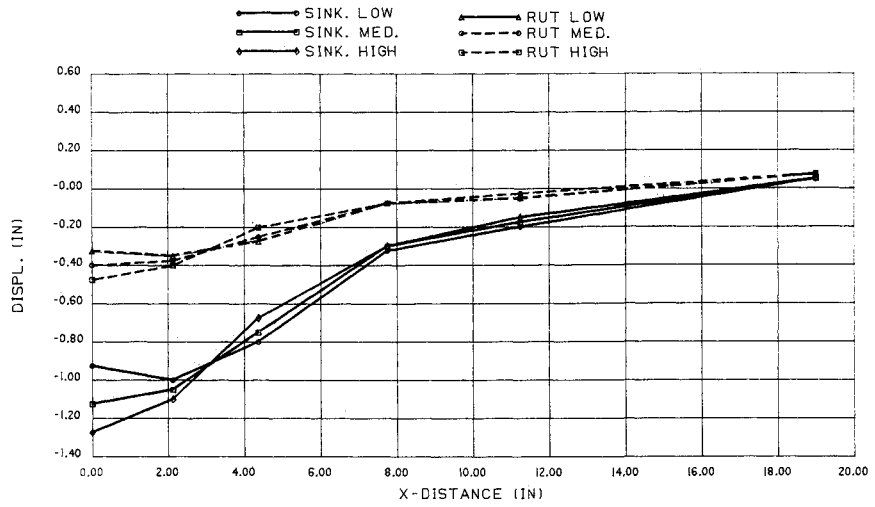

Fig. 6 Sinkage and rut depth for three tire pressures on sand.

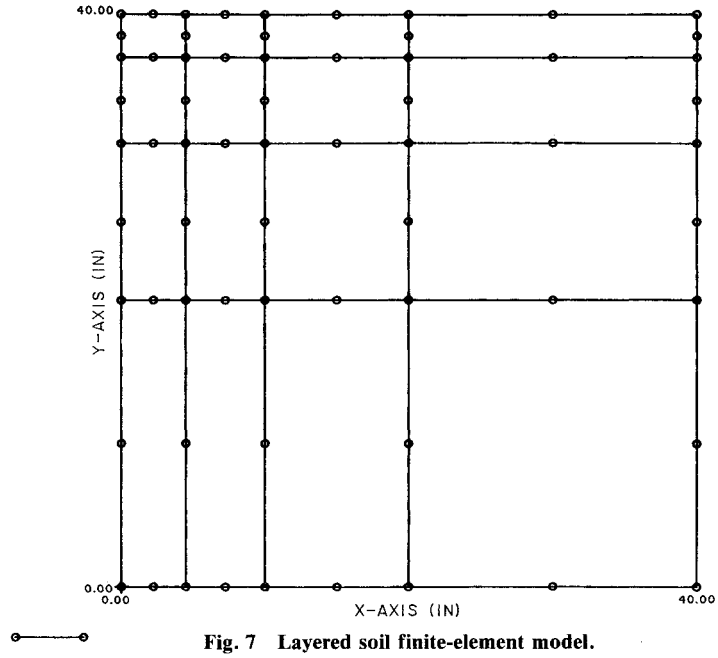

Fig. 7 Layered soil finite-element model.

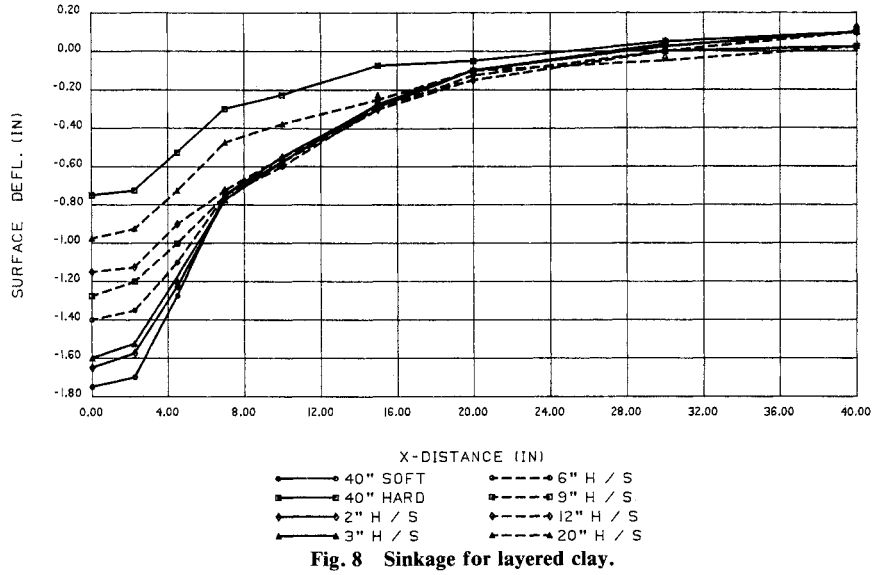

Fig. 8 Sinkage for layered clay.

sociated flow rule is used, the plastic potential function Q is similar to the yield function but with a different friction angle. The load is applied in increments of 0.6, 0.2, 0.1, 0.1, and -1 times the maximum pressure, thus modeling a one pass phenomenon over that strip of soil. The results of this study are shown in Figs. 5 and 6 where the sinkage and rut depth of the top surface are plotted for the three different tire pressures over the clay and sand soils.

V. Effect of Layered Soil on Sinkage and Rut Depth

The next problem attempted was to predict tire sinkage and rut depth resulting from a medium pressure tire traveling over clay and sand surfaces having two differnt layered strengths with the material properties shown in Table 2.

A medium tire pressure is assumed, and the finite-element model with all of the geometry is shown in Fig. 7. The top layer is assumed to be 3 in. thick, and the bottom layer is taken to be 37 in. A hard over soft as well as a soft over hard layer is examined, and the sinkage and rut depth for the top surface are plotted in Fig. 8 for clay and Fig. 9 for sand. Note that the same parameters for constant soft and hard layers of the same soil are also plotted on the same graph to correlate better the effect of layered soil

VI. Effect of the Top Thickness Layer on Sinkage

The Fig. 7 finite-element model was used to study the effect of the top layer thickness on soil behavior. The effect of a soft layer on top of a hard one is not a problem as can be seen in the previous two graphs. In contrast, the behavior of a hard layer on top of a soft one is much more complex and more common in practice. This case was examined by varying the top thickness by making it 2, 3, 6, 9, and 20 in. thick. The resulting tire sinkages are shown for the clay soil in Fig. 10 and the sandy soils in Fig. 11.

VII. Equivalent Cone Index for an F-4 Tire on Clay

A cone index is an indicator of soil-shearing resistance obtained using a probe-type instrument designed to measure soil strength. It consists of a right circular cone with a 0.5-in.^{2} base area and is operated at a penetration rate of approximately 1.25 in./s.

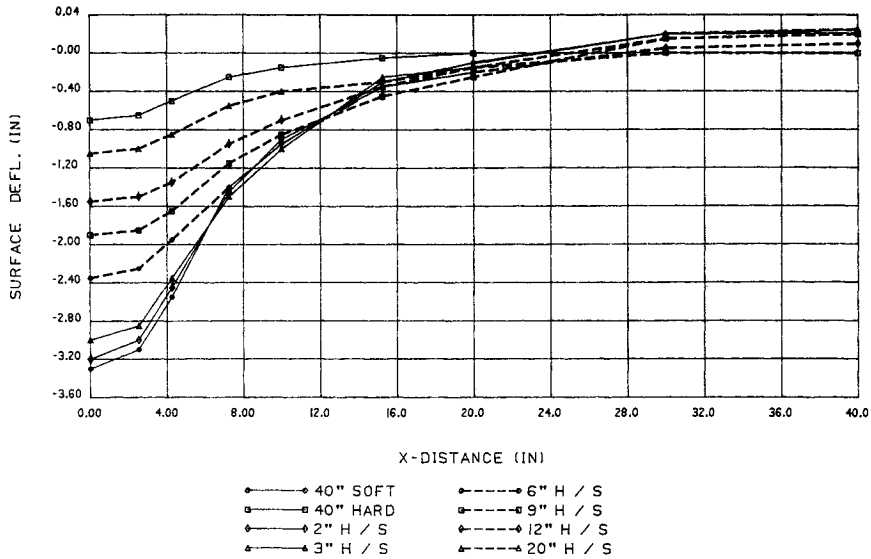

Fig. 9 Sinkage for layered sand.

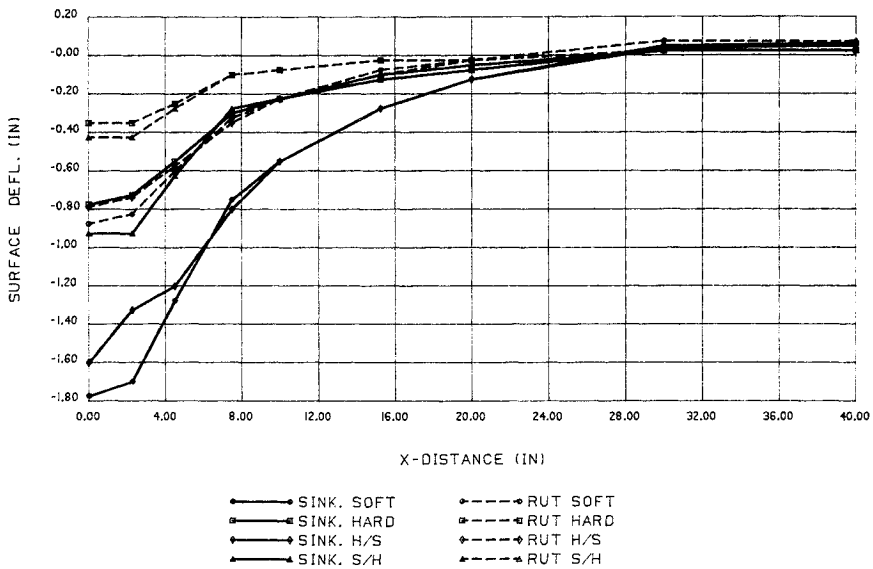

Fig. 10 Sinkage and rut depth for layered clay.

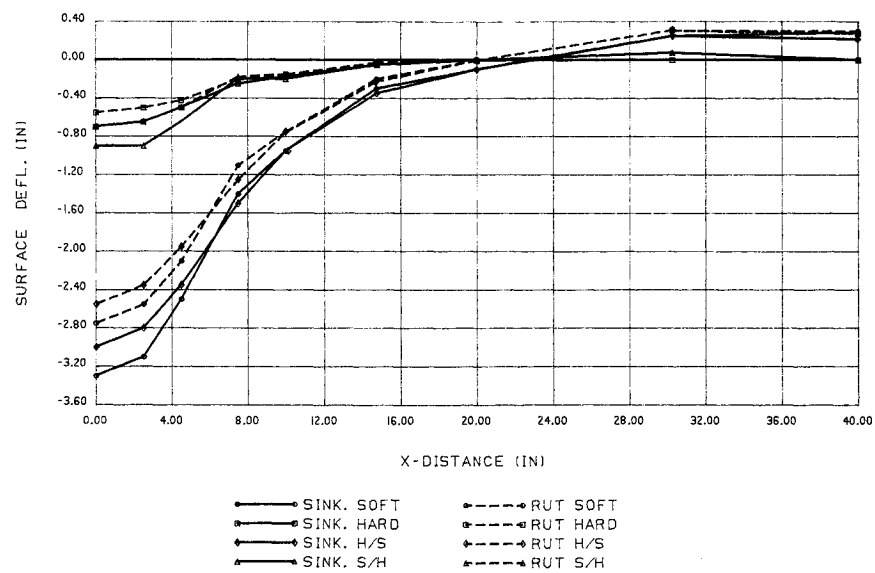

Fig. 11 Sinkage and rut depth for layered sand.

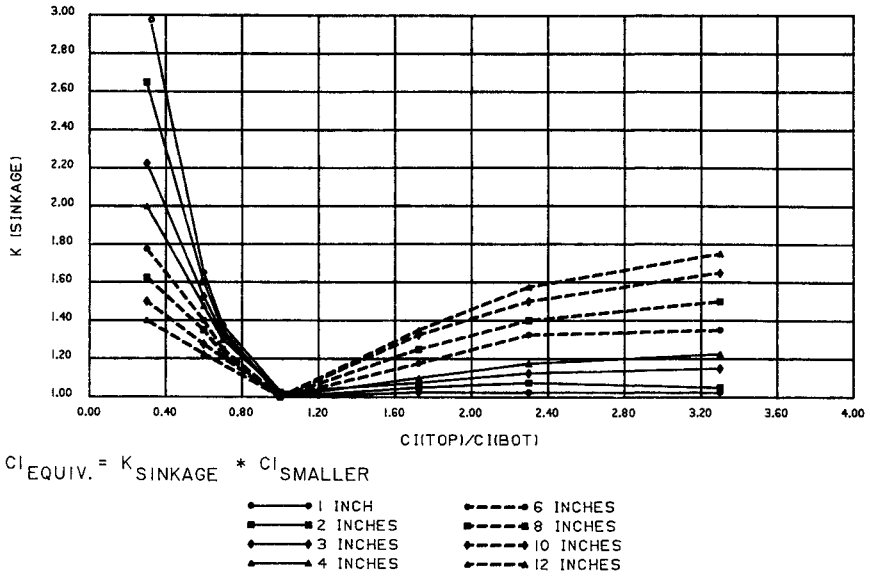

Fig. 12 Equivalent cone index for sinkage.

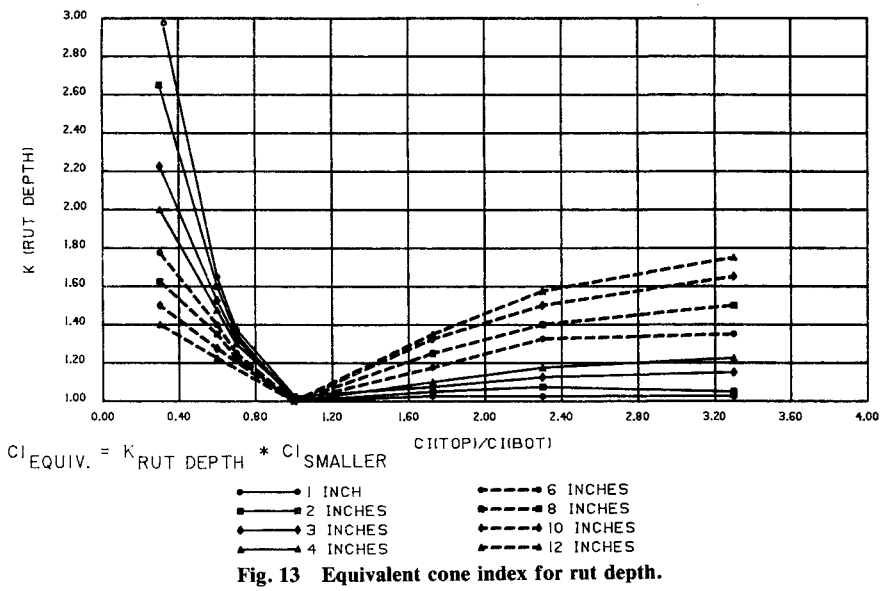

Fig. 13 Equivalent cone index for rut depth.

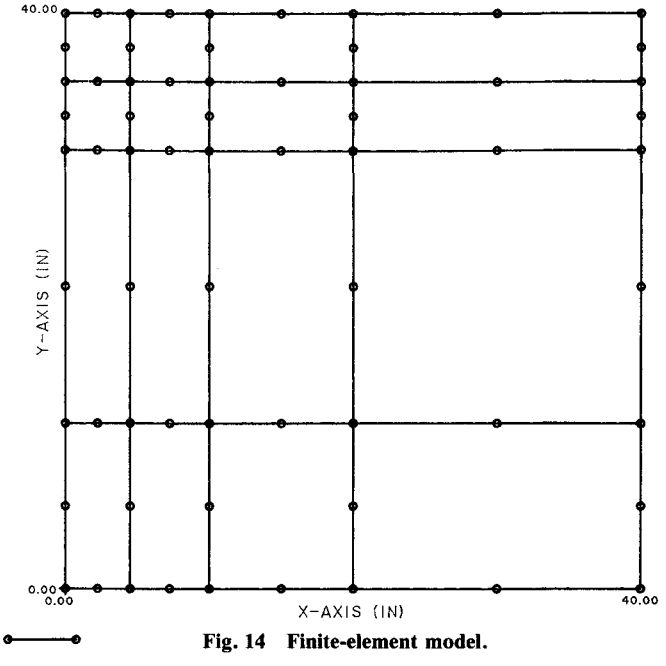

Fig. 14 Finite-element model.

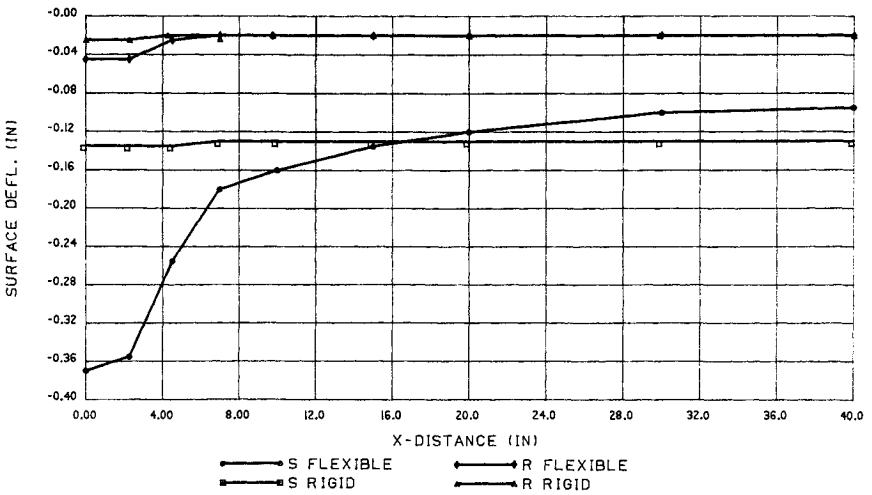

Fig. 15 Sinkage and rut depth for rigid and flexible pavements.

To compute an equivalent cone index for a two-layered soil of different strength and thickness, we first picked material properties such that both sinkage and rut depth from the finite-element program matched their respective experimental values[2] for cone indexes of 240, 320, 400, 480, 560, 640, 720, and 800. Then all of the possible combinations of ratios with cone index 240 were considered, and the sinkage and rut depth were computed for top thicknesses of 1, 2, 3, 4, 6, 8, 10, and 12 in. keeping the total thickness constant and equal to 40 in. Then the computed sinkages and rut depths were matched again with experimental values,[2] and an equivalent cone index was selected. This equivalent cone index was then divided by 240 and a dimensionless K constant was obtained. The summary of this study is shown in Figs. 12 and 13.

VIII. Sinkage and Rut Depth for Flexible and Rigid Pavements

Finally, a very weak theoretical, flexible, and rigid pavement under a medium pressure tire were considered. The pavement was assumed to be composed of 9½ in. of a weak asphalt concrete or a Portland Cement concrete on top of 19 in. of crushed limestone on top of a layer of clay. Average published values were used to establish the material properties used, which are shown in Table 3.

The finite-element model for this study is shown in Fig. 14. Figure 15 shows the predicted tire sinkages and rut depths.

IX. Conclusions

The developed theoretical technique and the resulting finite-element program provide a powerful analytical tool and hold significant promise to improve USAF ability to predict aircraft ground operation.

This viscoplastic finite-element program uses classic constitutive relations and state-of-the-art numerical techniques to model soil. It is capable of providing urgently needed improvements for predicting aircraft tire sinkage and rut depth on soils or any contingency/austere surface. This study has demonstrated that the computer program has potential to improve significantly the reliability and accuracy for predicting aircraft operation on soil surfaces having large variations in strength with depth. This study also showed that the analysis precedure can be adapted to provide a basis for predicting aircraft operation on other contingency surfaces.

Acknowledgments

The author would like to acknowledge the Air Force Systems Command, Air Force Office of Scientific Research, and the Flight Dynamics Laboratory for their sponsorship of this program. The author would also like to thank Mr. George J. Sperry of AFWAL/FIEM for his help in contacting appropriate individuals and obtaining pertinent documentation and for his support and guidance.

References

[1]Kraft, D. C., and Hoppenjaus, J. R., "Aircraft Surface Operation Soil Surface Correlation Study," University of Dayton, Dayton, OH, AFFDL-TR-70-30, 1970.

[2]Luning, H., "Analytical Aircraft Landing Gear Soil Interaction Phase II, Rolling Single Wheel Analytical Sinkage Prediction Technique and Computer Program," University of Dayton, Dayton, OH, AFFDL-TR-71-142, 1971.

[3]Kraft, D., "Multiwheel Landing Gear—Soils Interaction and Flotation Criteria, Phase III," University of Dayton, Dayton, OH, AFFDL-TR-71-12, Pts. I and II, 1971.

[4]Kraft, D., "Landing Gear/STOL Interaction Development of Criteria for Aircraft Operation on Soil During Turning and Multi-Pass Operations," University of Dayton, Dayton, OH, AFFDL-TR-75-78, 1975.

[5]Phillips, N. S., and Saliba, J. E., "Landing Gear/Soil Interaction Development of Criteria for Aircraft Operation on Soil During Turning and High Speed Straight Roll Computer Programs Documentation Volume II," Air Force Flight Dynamics Laboratory, Wright-Patterson Air Force Base, OH, ASL-TR-82-29, June 1981.

[6]Saliba, J. E., "An Elastic-Viscoplastic Finite Element Model for Representing Layered Soils—Description Volume I," Air Force Engineering and Services Center, Tyndall Air Force Base, FL, AFESC/RDCR, Jan. 1984.

[7]Owen, D. R. J., and Hinton, E., *Finite Elements in Plasticity Theory and Practice,* Pineridge, Swansea, United Kingdom, 1980.

[8]Kanchi, M. B., Zienkiewicz, O. C., and Owen, D. R. J., "The Viscoplastic Approach to Problems of Elasticity and Creep Involving Geometric Nonlinear Effects," *International Journal of Numerical Methods Engineering,* Vol. 12, 1978, pp. 169-181.

[9]Stricklin, J. A., Haisler, W., and Reisemann, W., "Evaluation of Solution Procedures of Material and/or Geometrically Nonlinear Structural Analysis," *AIAA Journal,* Vol. 11, 1973, pp. 292-29.

[10]Saliba, J. E., "Numerical Stability of Implicit Integration Schemes in Nonassociated Viscoplasticity," Ph.D. Dissertation, University of Dayton, Dayton, Ohio, 1983.